JOURNAL OF MATERIALS SCIENCE 17 (1982) 3101–3105

Zr–Hf interdiffusion in polycrystalline Y_2O_3–(Zr + Hf)O_2

Y. SAKKA, Y. OISHI, KEN ANDO
Department of Nuclear Engineering, Kyushu University, Fukuoka 812, Japan

Lattice and grain-boundary interdiffusion coefficients were calculated from the concentration distributions determined for Zr–Hf interdiffusion in polycrystalline $16Y_2O_3 \cdot 84(Zr_{1-x}Hf_x)O_2$ with $x = 0.020$ and 0.100. The lattice interdiffusion coefficients were described by $D = 0.031 \exp[-391\,(\text{kJ mol}^{-1})/RT]\ \text{cm}^2\ \text{sec}^{-1}$ and the grain-boundary diffusion parameters by $\delta D' = 1.5 \times 10^{-6} \exp[-309\,(\text{kJ mol}^{-1})/RT]\ \text{cm}^3\ \text{sec}^{-1}$ in the temperature range 1584–2116° C. Comparison of the results with those for the systems CaO–(Zr + Hf)O_2 and MgO–(Zr + Hf)O_2 indicated that the Zr self-diffusion coefficient was insensitive to the dopants in the fluorite–cubic ZrO_2 solid solutions.

1. Introduction

Solid solutions of ZrO_2 with MgO, CaO, and Y_2O_3 exhibit wide composition–temperature ranges in which a single fluorite–cubic phase is stable [1–3]. In these solid solutions, the oxygen vacancy concentration is known to be proportional to the concentration of the dopant ions substituted for Zr ions. This results in high diffusion coefficients of the oxygen ions, which lead to high ionic conductivities of stabilized zirconias [4]. Electrical conductivities of stabilized zirconias have been widely studied, but direct determinations of self-diffusion coefficients of the constituent ions have been conducted only for limited systems. Rhodes and Carter determined cation diffusion coefficients in the CaO–ZrO_2 system by tracer techniques and reported that the Zr self-diffusion coefficients did not significantly differ between 12 and 16 mol% CaO-stabilized zirconias but were much lower than the oxygen self-diffusion coefficient [5]. The present authors determined the Zr–Hf interdiffusion coefficients in $16CaO \cdot 84(Zr_{1-x}Hf_x)O_2$ which was produced by partial substitution of HfO_2 for ZrO_2 in the CaO-stabilized zirconia and found that the Zr–Hf interdiffusion coefficients were close to the Zr self-diffusion coefficients in $16CaO \cdot 84ZrO_2$. The results were interpreted that the self-diffusion coefficients of the Zr ion and the Hf ion were similar and that Hf may be regarded as the tracer for determination of the Zr self-diffusion coefficient in the CaO-stabilized zirconia. The Zr–Hf interdiffusion coefficient similarly determined for $14MgO \cdot 86(Zr_{1-x}Hf_x)O_2$ was also close to the Zr tracer diffusion coefficient in CaO–ZrO_2 [6].

In the present study, the Zr–Hf interdiffusion coefficients in Y_2O_3–ZrO_2–HfO_2 were determined in order to clarify how a trivalent dopant, replacing the divalent dopants, affects the Zr diffusion coefficient in stabilized zirconias. The Zr–Hf interdiffusion coefficient to be determined here is interpreted as the Zr self-diffusion coefficient for the Y_2O_3–ZrO_2 solid solution by analogy with CaO–ZrO_2 and MgO–ZrO_2.

Cation diffusion is expected to be enhanced by grain boundaries in Y_2O_3–ZrO_2–HfO_2, as is the case for CaO–ZrO_2 [5]. Lattice and grain-boundary interdiffusion coefficients are separately calculated in the present study, from the Zr and Hf concentration distributions determined in polycrystalline solid solution after interdiffusion. The results are compared with those of CaO–ZrO_2–HfO_2 and MgO–ZrO_2–HfO_2.

2. Experimental details

The Y_2O_3 content was fixed at 16.0 mol% in preparing a diffusion couple of two compositions, $16Y_2O_3 \cdot 84(Zr_{1-x}Hf_x)O_2$, in which the Hf fractions were designed to be $x = 0.020$ and 0.100. Appropriate mixtures of Y_2O_3 (99.99% purity), ZrO_2 (99.69% purity), and HfO_2 (99.95% purity) were isostatically pressed into a pellet shape of 10 mm diameter and 5 mm high under a pressure

0022–2461/82/113101–05$03.10/0

of 2×10^7 kg m^{-2}, and the pressed pellets were pre-sintered at 1300° C for 15 h in air. The pre-sintered pellets were sintered at 2200° C in vacuum for 3 to 6 h depending on the diffusion temperatures, and then annealed again in air at 1300–1400° C for over 3 h.

Formation of homogeneous single fluorite–cubic solid solution was confirmed by means of X-ray diffraction and electron probe microanalysis. The densities of the pellets ranged from 93 to 95% of the theoretical, as calculated with the assumption of substitutional solid solution of Y ions for Zr ions with formation of oxygen vacancies. The grain radii of the pellets, necessary to the present analysis, were determined using Fullman's relation [7].

Diffusion couples were prepared by joining two pellets with different Hf contents at 1600° C for 20 min in a molybdenum high-frequency induction furnace. Interdiffusion annealing was conducted in two ways. The 1584° C interdiffusion was conducted in air using an SiC furnace and inter-diffusions at 1885–2116° C in an Ar atmosphere using a W-mesh heater furnace.

After diffusion annealing, each diffusion couple was sawed into halves vertical to the interface. One half was used for measuring the grain size to confirm that no grain growth occurred during diffusion annealing. The other half was used for electron probe microanalysis. The detailed procedure of electron probe microanalysis was described elsewhere [6]. Determination of the chemical composition was carried out using a calibration chart assuming a quasi-binary diffusion; no up-hill diffusion of the Y ions occurred in the present ternary diffusion [8], since the diffusivities of the Zr and Hf ions were expected to be close [6].

3. Results

The concentration distribution for grain-boundary enhanced diffusion has been described by Oishi and Ichimura as a function of the lattice and grain-boundary diffusion coefficients by [9],

$$\frac{2(C-C_1)}{C_2-C_1} = \frac{M_t}{M_\infty}\exp(-my), \qquad (1)$$

where

$$\frac{M_t}{M_\infty} = 1-\frac{6}{\pi^2}\sum_{n=1}^{\infty}\frac{1}{n^2}\exp\left(-\frac{Dn^2\pi^2 t}{r^2}\right), \qquad (2)$$

$$m = \left[\frac{4D}{r\delta D'}\sum_{n=1}^{\infty}\exp\left(-\frac{Dn^2\pi^2 t}{r^2}\right)\right]^{1/2}, \qquad (3)$$

y is the diffusion distance from the interface, C the concentration at y, C_1 and C_2 the initial concentrations of the diffusion couple, M_t and M_∞ the diffusion amounts at times t and infinity, respectively, D and D' the lattice and grain-boundary diffusion coefficients, respectively, r the grain radius, and δ the grain-boundary thickness. Equation 1 can be rewritten as Equation 4 in a logarithmic form,

$$\ln\frac{2(C-C_1)}{C_2-C_1} = \ln\frac{M_t}{M_\infty} - my, \qquad (4)$$

which indicates that $\ln[2(C-C_1)/(C_2-C_1)]$ is proportional to the diffusion distance y.

An example of the $\ln[2(C-C_1)/(C_2-C_1)]$ plotted against y is shown in Fig. 1 for the diffusion couple of $16Y_2O_3 \cdot 84(Zr_{0.98}Hf_{0.02})O_2$ of average grain radius 32 μm and $16Y_2O_3 \cdot 84(Zr_{0.90}Hf_{0.10})O_2$ of average grain radius 31 μm after interdiffusion at 1885° C for 10 h. The satisfactorily linear relations indicate that the diffusion model represented by Equation 1 is applicable to the present interdiffusion. From the slopes and intercepts of the straight lines in Fig. 1, D and $\delta D'$ are separately calculated from Equations 2 and 3. A correction of the diffusion time was made in the calculation for the period of joining the diffusion couple as well as for increasing and decreasing the temperature before and after an isothermal diffusion annealing [9].

The D and $\delta D'$ thus determined are shown in

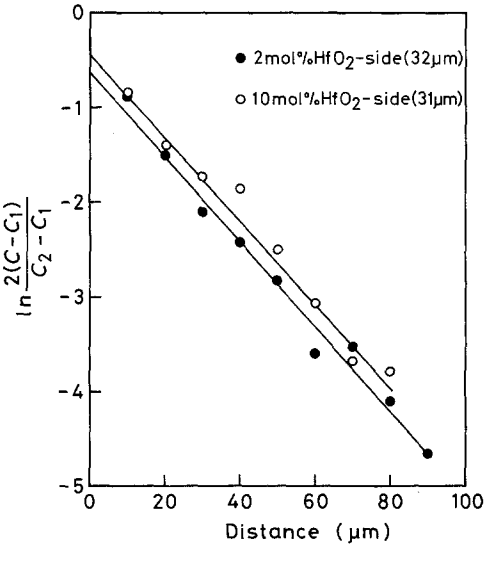

Figure 1 Logarithmic concentration distributions for the diffusion couple of $16Y_2O_3 \cdot 84(Zr_{0.98}Hf_{0.02})O_2$–$16Y_2O_3 \cdot 84(Zr_{0.90}Hf_{0.10})O_2$ at 1885° C for 10 h.

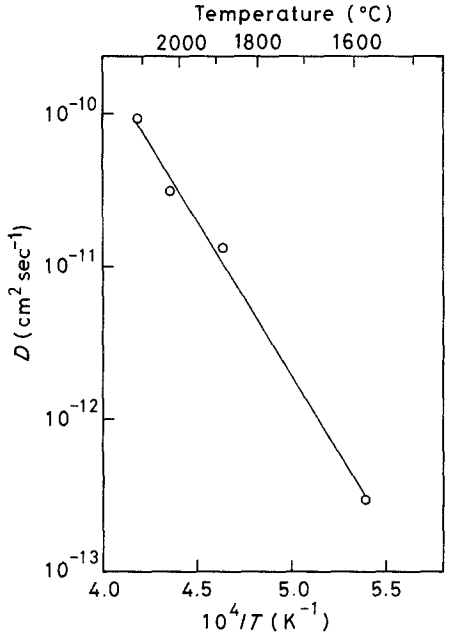

Figure 2 Lattice Zr–Hf interdiffusion coefficients for $16Y_2O_3 \cdot 84(Zr_{1-x}Hf_x)O_2$ as a function of temperature.

Figs 2 and 3, respectively, where the averages of the values obtained on both sides of the diffusion couples are plotted. Comparison of the results from diffusion anneals conducted in air (1584° C) and in an Ar atmosphere (above 1885° C) indicates no noticeable effect of the atmosphere on the results, as is the case for $CaO–(Zr + Hf)O_2$ and $MgO–(Zr + Hf)O_2$ [6].

Values of D and $\delta D'$ for the temperature range 1584–2116° C are described by Equations 5 and 6, respectively.

$$D = 0.031 \begin{matrix} + 0.047 \\ - 0.019 \end{matrix} \exp [-391 \pm 16\,(\text{kJ mol}^{-1})/RT]\ \text{cm}^2\ \text{sec}^{-1}, \quad (5)$$

$$\delta D' = \left(1.5 \begin{matrix} + 3.7 \\ - 1.1 \end{matrix}\right) \times 10^{-6} \exp [-309 \pm 22\,(\text{kJ mol}^{-1})/RT]\ \text{cm}^3\ \text{sec}^{-1}, \quad (6)$$

The activation energy of $\delta D'$ is approximately 80 kJ mol^{-1} smaller than that of the lattice interdiffusion.

4. Discussion

In Fig. 4, the determined D (Zr–Hf) in $16Y_2O_3 \cdot 84(Zr_{1-x}Hf_x)O_2$ is compared with those in $16CaO \cdot 84(Zr_{1-x}Hf_x)O_2$ and $14MgO \cdot 86(Zr_{1-x}Hf_x)O_2$ [6] and the Zr self-diffusion coefficients, D^*_{Zr}, in $12CaO \cdot 88ZrO_2$ and $16CaO \cdot 84ZrO_2$ [5]. The corresponding frequency factors and activation energies are listed in Table I. The close diffusion parameters in these

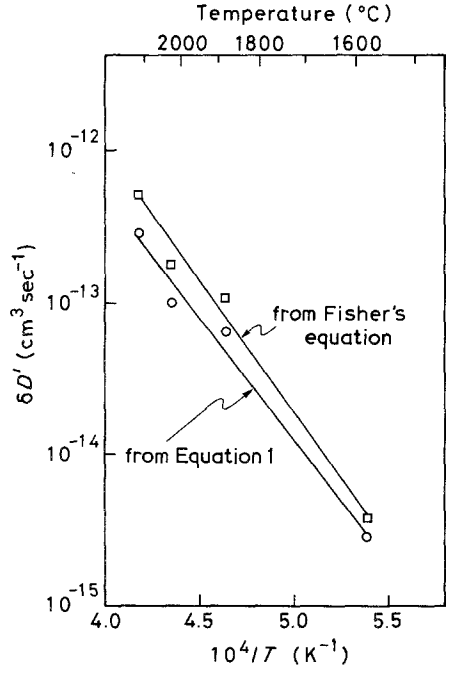

Figure 3 Grain-boundary diffusion parameters for $16Y_2O_3 \cdot 84(Zr_{1-x}Hf_x)O_2$ calculated from Equation 1 and from Fisher's equation as a function of temperature.

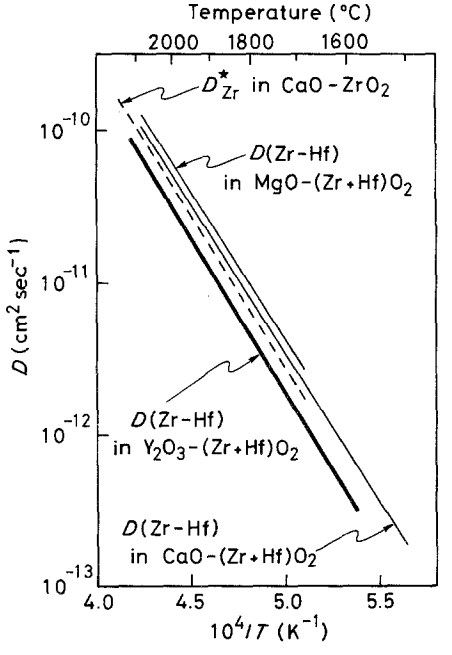

Figure 4 Comparison of lattice Zr–Hf interdiffusion coefficients for $Y_2O_3–(Zr + Hf)O_2$, $CaO–(Zr + Hf)O_2$, and $MgO–(Zr + Hf)O_2$ and Zr tracer diffusion coefficient for $CaO–ZrO_2$.

TABLE I Lattice diffusion parameters for Zr tracer diffusion and Zr–Hf interdiffusion in stabilized zirconias

Substance	Diffusion type	Temperature range (° C)	D_0 ($cm^2\ sec^{-1}$)	Q ($kJ\ mol^{-1}$)	Reference
$12CaO \cdot 88ZrO_2$ $16CaO \cdot 84ZrO_2$	D^*_{Zr}	1700–2150	0.035	387	[5]
$16CaO \cdot 84(Zr_{1-x}Hf_x)O_2$	D (Zr–Hf)	1502–2083	0.023	377	[6]
$14MgO \cdot 86(Zr_{1-x}Hf_x)O_2$	D (Zr–Hf)	1680–2083	0.033	381	[6]
$16Y_2O_3 \cdot 84(Zr_{1-x}Hf_x)O_2$	D (Zr–Hf)	1584–2116	0.031	391	This work

stabilized zirconias with and without HfO_2 substituted for ZrO_2 imply, according to Darken's relation, that the self-diffusion coefficients of Zr and Hf ions are similar and, consequently, D (Zr–Hf) in the ternary oxide systems can be regarded as the Zr self-diffusion coefficients in the corresponding binary solid solutions with no HfO_2 [6] and that the Zr self-diffusion coefficient in stabilized zirconia is not markedly influenced by the kind of dopant cation, and is not sensitive to the dopant concentration. (The Zr tracer diffusion coefficients in 12 and 16 mol% CaO-stabilized zirconias did not exhibit significant difference in the determination of Rhodes and Carter [5].)

As shown in Fig. 5, grain-boundary diffusion parameters seem to be similar in absolute magnitude for $16CaO \cdot 84(Zr_{1-x}Hf_x)O_2$, $14MgO \cdot 86(Zr_{1-x}Hf_x)O_2$ [6], and $16Y_2O_3 \cdot 84(Zr_{1-x}Hf_x)O_2$, and also for the Zr tracer diffusion in $CaO–ZrO_2$ (square) [5]. Explanation of the activation energy of $\delta D'$ in Y_2O_3–$(Zr + Hf)O_2$, higher by 50 kJ mol^{-1} than that in $MgO–(Zr + Hf)O_2$ and $CaO–(Zr + Hf)O_2$, requires details of the microstructures in the polycrystalline samples. Fig. 5 also shows the $\delta D'$ obtained from a creep experiment of tetragonal ZrO_2 (circle) [10]. This value is close to the extrapolated value of $\delta D'$ in the fluorite–cubic stabilized zirconias, suggesting similar grain-boundary diffusion characteristics of Zr ions in fluorite–cubic and tetragonal structures.

Fig. 3 shows the grain-boundary diffusion parameters calculated by Equation 1 and by Fisher's equation [11] from the same experimental data of the present work. The higher $\delta D'$ from Fisher's equation than from Equation 1, by a factor of two, is due to the present boundary condition where the diffusion distance is larger than the grain size. The smaller the grain size or the longer the diffusion time, the larger tends to be the difference between the two calculations. Since Fisher's equation* describes the diffusion flux only from the grain boundaries parallel to the diffusion direction, the ignored diffusion flux from the grain boundaries perpendicular to the diffusion direction results in an overestimated $\delta D'$ in the present case.

Acknowledgements

The authors acknowledge the assistance of Y. Ikeda and M. Masuda in the experimental work.

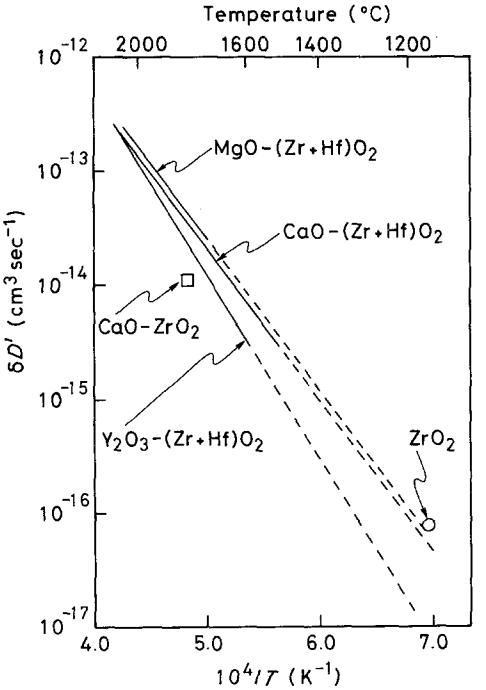

Figure 5 Comparison of $\delta D'$ for Y_2O_3–$(Zr + Hf)O_2$, $CaO–(Zr + Hf)O_2$, and $MgO–(Zr + Hf)O_2$ [6]. Squares denote the $\delta D'$ for Zr tracer diffusion in $CaO–ZrO_2$ [5]. Circles denote the $\delta D'$ obtained from creep experiments of tetragonal ZrO_2 [10].

*Whipple's equation [12] describes grain-boundary diffusion more accurately than Fisher's equation for the boundary condition of constant interface concentration. However, the present comparison is made with Fisher's equation which employs an approximated grain-boundary concentration distribution similar to that in Equation 1.

References

1. C. F. GRAIN, *J. Amer. Ceram. Soc.* **50** (1967) 288.
2. V. S. STUBICAN and S. P. RAY, *ibid.* **60** (1977) 534.
3. V. S. STUBICAN, R. C. HINK and S. P. RAY, *ibid.* **61** (1978) 17.
4. Y. OISHI, K. ANDO and M. AKIYAMA, *Nippon Kagaku Kaishi* (1981) 1445.
5. W. H. RHODES and R. E. CARTER, *J. Amer. Ceram. Soc.* **49** (1966) 244.
6. Y. OISHI, Y. SAKKA and K. ANDO, *J. Nucl. Mater.* **96** (1981) 23.
7. R. L. FULLMAN, *Trans. AIME* **197** (1953) 447.
8. Y. OISHI, *J. Chem. Phys.* **43** (1965) 1611.
9. Y. OISHI and H. ICHIMURA, *ibid.* **71** (1979) 5134.
10. B. BURTON, G. L. REYNOLDS and J. P. BARNES, *J. Nucl. Mater.* **98** (1981) 144.
11. J. C. FISHER, *J. Appl. Phys.* **22** (1951) 74.
12. R. T. P. WHIPPLE, *Phil. Mag.* **45** (1954) 1225.

Received 18 January
and accepted 1 March 1982